DOI:
10.1038/s41586-018-0032-3

Document Version
Peer reviewed version

An evolutionarily conserved ribosome-rescue pathway maintains epidermal homeostasis

Kifayathullah Liakath-Ali[1, #], Eric W. Mills[2], Inês Sequeira[1], Beate M. Lichtenberger[1, 3], Angela Oliveira Pisco[1], Kalle H. Sipilä[1], Ajay Mishra[1,4], Harunori Yoshikawa[5], Colin Chih-Chien Wu[2], Tony Ly[5, 6], Angus I Lamond[6], Ibrahim M. Adham[7], Rachel Green[2] and Fiona M. Watt[1]

1. Centre for Stem Cells and Regenerative Medicine, King's College London, 28th floor, Guy's Tower Wing, London SE1 9RT, UK.
2. Howard Hughes Medical Institute, Johns Hopkins School of Medicine, Department of Molecular Biology and Genetics, Baltimore, MD 21205, USA.
3. Skin & Endothelium Research Division, Department of Dermatology, Medical University of Vienna, Lazarettgasse 14, 1090 Vienna, Austria
4. Cambridge Infinitus Research Centre, University of Cambridge, Cambridge, UK
5. Centre for Gene Regulation and Expression, School of Life Sciences, University of Dundee, Dow Street, Dundee, DD1 5EH, Scotland, UK.
6. Wellcome Trust Centre for Cell Biology, University of Edinburgh, Michael Swann Building, King's Buildings, Edinburgh EH9 3BF, Scotland, UK.
7. Institute of Human Genetics, University Medical Centre of Göttingen, D-37073 Göttingen, Germany.

\# Present address: Department of Molecular and Cellular Physiology and Howard Hughes Medical Institute, Stanford University Medical School, 265 Campus Drive, CA 94305-5453, USA

Address for communication: fiona.watt@kcl.ac.uk

Ribosome-associated mRNA quality control mechanisms ensure fidelity of protein translation[1,2]. Although extensively studied in yeast, little is known about their role in mammalian tissues, despite emerging evidence that stem cell fate is controlled by translational mechanisms[3,4]. One evolutionarily conserved component of the quality control machinery, *Dom34/Pelota (Pelo),* rescues stalled ribosomes[5]. Here we show that *Pelo* is required for mammalian epidermal homeostasis. Conditional deletion of *Pelo* in those murine epidermal stem cells that express Lrig1 results in hyperproliferation and abnormal differentiation. In contrast, deletion in Lgr5+ stem cells has no effect and deletion in Lgr6+ stem cells has only a mild phenotype. Loss of *Pelo* results in accumulation of short ribosome footprints and global upregulation of translation rather than affecting expression of specific genes. Translational inhibition by rapamycin-mediated down regulation of mTOR rescues the epidermal phenotype. Our study reveals a novel role for the ribosome-rescue machinery in mammalian tissue homeostasis and an unanticipated specificity in its impact on different stem cell populations.

Pelo is expressed in mouse skin dermis and epidermis[6] (Extended Data Fig. 1a). Dermal-specific deletion (*Pelo*^{derKO}) resulted in mice that were smaller than littermate controls but had a normal lifespan and no dermal abnormalities (Fig. 1a-f). Although Dom34 forms a functional complex with Hbs1 in yeast[7] and the mammalian homolog *Hbs1l* is expressed in mouse skin[6] (Extended Data Fig. 1b), the *Hbs1l* knockout (from exon 5; Extended Data Fig. 1c) had no epidermal defects (Extended Data Fig. 1d-f) and only small changes in dermal collagen deposition, thickness and cell density (Extended Data Fig. 1f-m). Another Pelo partner, Gtpbp2[8], does not have a reported skin phenotype.

Selective embryonic deletion of *Pelo* in Krt14 expressing epidermal cells, comprising the known stem cell subpopulations[9], via *Krt14*^{Cre} (*Pelo*^{epiKO}; Fig. 1g) phenocopied deletion via the ubiquitous Rosa26 locus[10]. Mice were born with scaly skin and an epidermal barrier defect (increased trans epidermal water loss; TEWL). They exhibited hair and weight loss, failing to thrive beyond 5 months (Fig. 1h-k). Epidermal thickening resulted from increased proliferation (Fig. 1l-s) and abnormal accumulation of differentiated cells (Fig. 1n-t). Wound closure was delayed (Fig. 1u), correlating with reduced proliferation, differentiation and migration (Extended Data Fig. 2a-i). Hyperproliferation in unwounded skin combined with delayed wound healing and abnormal differentiation has been observed in other mouse models[11]. There was also striking degeneration of the sebaceous glands and hair follicles, correlating with loss of the hair follicle bulge stem cell markers Krt15 and CD34 and the junctional zone stem cell marker Lrig1 (Extended Data Fig. 3a-c).

To determine whether the *Pelo* epidermal phenotype could be induced postnatally, we applied 4-OHT to adult *Pelo*$^{fl/fl}$; *Krt14*^{CreERT} (Extended Data Fig. 4a, b). Mice developed skin lesions, increased TEWL and delayed wound closure (Extended Data Fig. 4c-e). Degeneration of hair follicles and sebaceous glands correlated with keratinized cyst formation (Extended Data Fig. 4f, g). Sebocyte differentiation was disturbed, accompanied by expansion of Lrig1 labelling into the upper sebaceous gland (Extended Data Fig. 4h, i).

PELO knockdown in cultured human epidermal keratinocytes led to an increase in stem cell colonies (Extended Data Fig. 5a-g). Immunostaining of epidermis reconstituted on decellularised dermis revealed increased proliferation of basal layer cells and increased differentiated layers

(Extended Data Fig. 5h-l). Therefore the mouse epidermal Pelo phenotype was recapitulated in human cells.

To determine if there is a differential requirement for *Pelo* in different epidermal subpopulations, we conditionally deleted *Pelo* in Lgr5+, Lgr6+ and Lrig1+ stem cells (Fig. 2a-c). *Pelo* deletion in Lrig1+ cells recapitulated the effects of deleting *Pelo* in Krt14+ cells, whereas when *Pelo* was deleted in Lgr5+ and Lgr6+ cells differentiation was normal (Fig. 2d) with only a small increase in Ki67+ cells (Extended Data Fig. 5m, Fig. 2f). *Pelo* deletion in Lrig1+ cells increased cell proliferation in the upper hair follicle, with marked changes in follicles and sebaceous glands (Fig. 2e, Extended Data Fig. 6a, b). A significant increase in proliferation and TEWL occurred in the interfollicular epidermis (IFE) of $Pelo^{fl/fl}$; $Lrig1^{CreERT2}$ mice compared to $Pelo^{fl/fl}$; $Lgr5^{CreERT2}$ and $Pelo^{fl/fl}$; $Lgr6^{CreERT2}$ mice (Extended Data Fig.5m, Fig. 2f, h). There was a small increase in epidermal thickness in $Pelo^{fl/fl}$; $Lgr6^{CreERT2}$ mice but TEWL was unaffected (Fig. 2g, h).

We next generated $Pelo^{fl/fl}$; $Lrig1^{CreERT2}$; $Rosa26^{tdTom}$, $Pelo^{fl/fl}$; $Lgr5^{CreERT2}$; $Rosa26^{tdTom}$, and $Pelo^{fl/fl}$; $Lgr6^{CreERT2}$; $Rosa26^{tdTom}$ mice, and treated with 4-OHT. *Pelo* deletion did not change the contribution of Lgr5 or Lgr6 progeny to the epidermis (Extended Data Fig. 6c, d). In contrast, on *Pelo* deletion Lrig1 lineage cells expanded downwards into the hair follicles and fully colonized the IFE (Extended Data Fig. 6c, d). In the presence or absence of Pelo, the Lrig1 lineage accounted for most Ki67+ epidermal cells; they also accounted for the increase in proliferative cells on *Pelo* deletion (Extended Data Fig. 6e, f).

Yeast cells lacking *Dom34* (the homolog of *Pelo*) are enriched in short 16-18 nucleotide ribosome-protected fragments (RPFs) resulting from translation to the 3′end of truncated mRNAs[5]. *Dom34/Rli1* mutant yeast accumulate full length 28-32 nucleotide RPFs in 3′ UTRs, consistent with the role of *Dom34* and *Rli1* in ribosome rescue and recycling on intact mRNAs, respectively[12]. In anucleate hematopoietic cells PELO and ABCE1 (Rli1) rescue non-translating 3′UTR ribosomes[13] and impact mRNA stability[14]. When we performed ribosomal profiling on keratinocytes from adult *Pelo*^{epiKO} mice by deep sequencing RPFs[15], RPFs mapped primarily to the coding sequence (CDS) (Fig. 3a; Extended Data Fig. 7a, b), consistent with studies[12] showing that loss of PELO alone does not substantially increase 3′ UTR ribosomes. CDS RPFs were primarily 28-34nts, the expected fragment size protected by mammalian ribosomes[16], and displayed the three-nucleotide periodicity reflecting codon-by-codon movement of elongating ribosomes (Fig. 3b, gray bars).

Pelo^{epiKO} profiles were enriched in 20-21 nucleotide RPFs (~4-5% of total RPFs compared to <1% in control cells) (Fig. 3a-c). Like the dominant population of 28-34nt RPFs, these footprints were primarily found in the CDS and showed a strong reading frame signal, indicating they too reflect the presence of elongating ribosomes, yet are shortened on their 3′ end after nuclease digestion (Fig. 3d, right). The density of short RPFs was evenly distributed and did not increase in frequency near the downstream 3′ portion of transcripts (Fig. 3a), as would be anticipated if they resulted from ribosomes encountering a directional RNA decay process[17,18]. Consistent with this, enrichment for 20-21 nt footprints was not linked to reduced transcript abundance in *Pelo*^{epiKO} cells (Fig. 3e; Supplementary Table 1). While Pelo is implicated in decay of the unusual histone mRNAs that lack polyA tails[19], the short footprints did not demonstrate patterns

to indicate they result from ribosomes occupying transcripts that are being degraded. The 21mer RPFs seen in *Pelo*^{epiKO} cells could be the equivalent of the 16mer species in yeast[5] and reflect the increased size of the mammalian ribosome[20]. However, we suggest they are equivalent to the 21nt fragments observed[21] in anisomycin-treated yeast cells and reflect dependence on Pelo-associated quality control mechanisms in response to tRNA starvation in rapidly dividing cells.

Epidermal *Pelo* loss led to significant changes in global translational efficiency (TE)[15] (Fig. 3f, g; $p < 0.01$). TE values for keratins and ribosomal proteins were notably increased (Fig. 3f, g). There was significant enrichment for genes involved in RNA metabolism, protein synthesis, extracellular matrix and chromatin regulation (Fig. 3h; Extended Data Fig. 7c to e; Supplementary Table 2; Supplementary Table 3). There was also differential expression of canonical translational pathways, including upregulation of the mTOR (mechanistic target of rapamycin) pathway (Fig. 3h; Extended Data Fig. 8a, b). Since mTOR signaling leads to increased global translation[22] (Extended Data Fig. 8c), we compared the Gtpbp2/tRNA mutant[8] and *Pelo*^{epiKO} gene expression datasets. We found significant overlap in translational signaling pathways (Extended Data Fig. 8d), suggesting that ribosome stalling is sensed by mTOR.

The polysome-to-monosome ratio was increased in *Pelo*^{epiKO} cells (Fig. 3i), suggesting an overall increase in translation or accumulation of inactive stalled ribosomes. *Krt86* transcripts were enriched in the heavy polysome fractions (Fig. 3j), consistent with the increases in TE values, suggesting increased overall translation. This was confirmed by quantifying global protein synthesis by O-propargyl-puromycin (OP-P) incorporation into newly synthesized polypeptide chains[3,4]. OP-P incorporation was increased in *Pelo*^{epiKO} IFE and hair follicles compared to

142 controls. Labelling was higher in the IFE suprabasal than basal layer, consistent with increased
143 total protein synthesis during differentiation (Fig. 4a-d)[23]. The increase in OP-P labelling in total
144 *Pelo* null keratinocytes (Fig. 4e) and stem cells (Integrin α6-high cells; Itga6^{high}) was confirmed
145 by flow cytometry (Extended Data Fig. 9a, Fig. 4f-j). Confocal microscopy revealed a striking
146 increase in the size of *Pelo*^{epiKO} basal cells (Extended Data Fig. 9b-d), consistent with increased
147 protein synthesis and a higher proportion of G2/M and S phase cells (Extended Data Fig. 9e).
148
149 In control mice, Lrig1+ cells exhibited slightly higher protein synthesis than Lgr5 and Lgr6+
150 cells (Fig. 4k, l). When *Pelo* was deleted, protein synthesis in Lrig1+ cells was increased further
151 relative to Lgr5 and Lgr6+ cells (Fig. 4k, l). RNA-seq (Extended Data Fig. 10a) revealed that
152 regardless of whether or not *Pelo* was expressed, Lgr5+ cells clustered separately from Lrig1+
153 and Lgr6+ cells, while the gene expression profiles of individual populations did not cluster
154 based on *Pelo* expression (Extended Data Fig. 10b-j, Supplementary Tables 4, 5). Therefore the
155 *Pelo* epidermal phenotype primarily reflects increased translation, rather than expression of
156 specific genes.
157
158 To downregulate mTOR1[22], we applied rapamycin to adult *Pelo*^{epiKO} skin (Extended Data Fig. 9f,
159 g). There was a significant reduction in Ki67+ cells compared to controls (Extended Data Fig.
160 9h-j). Phosphorylated ribosomal protein S6K (pS6K), a key substrate of mTOR[22], was increased
161 in *Pelo*^{epiKO} skin, and reduced by rapamycin (Extended Data Fig. 9k). However, rapamycin did
162 not prevent disruption of hair follicle and sebaceous gland architecture (Extended Data Fig. 9h).
163

Simultaneous rapamycin treatment and *Pelo* deletion largely prevented *Pelo*-mediated disruption of epidermal homeostasis (Fig. 4m, n). TEWL, epidermal thickening and proliferation were substantially reduced (Fig. 4o-u; Extended Data Fig. 9l); pS6K labeling was reduced (Fig. 4v) and phosphorylation of another mTOR substrate, 4EBP1, was decreased (Extended Data Fig. 9m). Therefore the epidermal *Pelo* deletion phenotype is largely attributable to increased protein translation.

Our results indicate that translational control is critical for tissue homeostasis[3,4,13] and establish a link between *Pelo* inactivation and translational activation via mTOR. mTOR is known to regulate cell growth and proliferation[22,24] and is activated upon ribosome-stalling by Fragile X Mental Retardation Protein[25,26]. Impaired ribosomal biogenesis also activates mTOR1 signaling and stimulates translation initiation and elongation factors[27]. mTOR signaling may be activated to enhance the efficiency of the translational machinery in order to compensate for impaired or reduced availability of ribosomes[8,28].

The increased size of *Pelo*-null epidermal cells as a result of increased protein synthesis[23,30] may stimulate differentiation through decreased basement membrane engagement[29] and thus indirectly promote proliferation. Factors that may account for the selective sensitivity of Lrig1+ cells to Pelo deletion include their proliferative state, abundance and location relative to Lgr5+ and Lgr6+ cells, together with their known ability to repopulate different epidermal compartments[31].

Acknowledgements

We dedicate this work to Wolfgang Engel. FMW gratefully acknowledges funding from the Wellcome Trust and UK Medical Research Council. We are also grateful for funding from the Department of Health via the National Institute for Health Research comprehensive Biomedical Research Centre award to Guy's & St Thomas' National Health Service Foundation Trust in partnership with King's College London and King's College Hospital NHS Foundation Trust. RG acknowledges funding from Howard Hughes Medical Institute. TL is supported by Sir Henry Dale Fellowship (206211/Z/17/Z). We thank Dr. Christopher Lelliott and Valerie Vancollie for providing *Hbs1l* knockout samples, Drs. Aamir Ahmed, Giacomo Donati, Ryan Driskell, Shukry Habib, Magnus Lynch, Benedicte Oules, D. V. Krishna Pantakani, Ignacio Sancho-Martinez and all Wattlab members for helpful discussions. Technical help from Mr. Matteo Battilocchi, Mr. Chaozheng Li and staff at the Nikon Imaging Centre and the Hodgkin Biological Services Facility, King's College London is gratefully acknowledged. We thank the High-Throughput Genomics Group at the Wellcome Trust Centre for Human Genetics, Oxford, UK (funded by Wellcome Trust: 203141/Z/16/Z) for generation of the sequencing data.

Author contributions

KL and FMW conceptualized and led the study. KL, IS and BML performed and analysed mouse experiments. KHS and AJ performed and analysed cell culture experiments. AOP analysed data from ribosome profile and RNA-seq experiments. IMA generated the *Pelo* conditional knockout mouse. EWM, CCW and RG generated and analysed ribosome-profiling data. HY, TL and AIL generated and analyzed polysome data. KL and FMW wrote the manuscript with input from all authors.

Author Information

Authors declare no competing financial interests. Correspondence and requests should be addressed to Fiona Watt (Fiona.watt@kcl.ac.uk).

Fig. 1. Differential effects of *Pelo* deletion *Pelo*^{derKO} (a-f) and *Pelo*^{epiKO} (g-u) mice. (h) Arrows: skin abnormalities. (c, d, l, m) H&E staining of back (c, d) and tail (l, m) skin. Dermal cellularity (d) and epidermal thickness (m) were measured. n=12 sections analyzed over 3 mice per group. (e, f, n, p-r) Immunolabelling of sections (e, f, n, p) and wholemounts (q, r). Asterisks: non-specific; arrow: suprabasal labelling; dashed lines: epidermal-dermal boundary. (m, n) ***p<0.001, n=3 mice. (i) Kaplan-Meier curves (n=29 mice). (j) Body weight: ***p<0.0003; n=5 per group. (k) TEWL. p<0.05; n=3. (s) Quantification of proliferation. **p=0.0086; ***p=0.0003 for Ki67; 0.0006 for EdU; n=3. (t) Cumulative mean values of gene expression from ribosome profiling. (u) Wound closure. *p=0.0500; n=3. Representative images in 1c, e-f, l, p-r from 3 independent experiments. Ctrl: littermate controls. Scale bars 100 μm.

Fig. 2. Lrig1+ stem cells account for *Pelo* mutant epidermal phenotype (a-c) Schematics of *Lrig1*, *Lgr5* and *Lgr6* expression (a), breeding (b) and 4-OHT treatment (c). (d, e) Immunostaining of dorsal skin IFE sections (d) and tail wholemounts (e) with antibodies to the markers shown. (e) Asterisk: altered SG; arrow: altered JZ. (g-i) Quantification of proliferation (f), epidermal thickness (g) and TEWL (h). IFE, interfollicular epidermis; Inf, infundibulum; SG, sebaceous gland; JZ junctional zone; Bu, bulge; HG, hair germ. Scale bars 50 μm (d, f); 100 μm (e). Dashed lines: epidermal-dermal boundary. ***p=0.0010 (g, p63); ***p=0.0005; *p=0.0330,

232 $^{**}p$ = 0.0071 (g, Ki67); $^{**}p$=0.0083 (g, EdU). $^{**}p$=0.0044, 0.0011 (h). $^{*}p$=0.0167 (i), n=16
233 sections and wholemounts analyzed over 4 mice per group. n.s., non significant.
234
235 **Fig. 3. Accumulation of short ribosome footprints and global translational changes in *Pelo***
236 **knockout epidermis** (a) Metagene analysis of full length and short RPFs near the start (left) and
237 stop (right) codons. (b) RPF read length distributions. (c) Empiric cumulative distribution plot of
238 global enrichment of short 20-21nt relative to expected 28-34nt reads. (d) Designations of -15
239 peaks indicate positions of 5′ end of RPF; corresponding P site occupancy shown. (e) Relative
240 enrichment of short RPFs (y-axis) and change in RNA transcript levels (x-axis). (f) Replicate
241 analysis of translational efficiency (TE). (g) MA plot showing observed and expected variance in
242 TE measurements; p-adjusted <0.01, blue transcripts. (h) Canonical pathways linked to
243 translation regulation in *Pelo*^{epiKO}. (i) Epidermal polysome profiling. (j) qRT-PCR shows
244 significant increase in heavy polysome bound *Krt86* mRNA; p=0.019.
245
246 **Fig. 4. Inhibition of mTOR pathway attenuates Pelo phenotype progression** (a-d, r, t, v)
247 Immunolabelling for markers indicated. (s, u) Quantitation: $^{**}p$=0.0064 (s); $^{***}p$=0.0006 (u).
248 (b-l) OP-Puro injected newborn (b-j) and adult (k, l) mice. (e-k) Representative flow histograms
249 and (i, j, l) quantitation; n=3 mice per group. $^{*}p$=0.0406 (i), 0.0357 (j), 0.0198 (l). (m-v) 4-OHT
250 and rapamycin (Rapa) treatment. (o) TEWL; $^{*}p$=0.0145. (p, q) H&E stained dorsal skin.
251 $^{*}p$=0.0286. Scale bars 50 μm (a); 100 μm (b-d; p, r, s, v), n=12 sections and wholemounts
252 analyzed over 4 mice per group per group.
253
254

References

1 Brandman, O. & Hegde, R. S. Ribosome-associated protein quality control. *Nat Struct Mol Biol* **23**, 7-15, doi:10.1038/nsmb.3147 (2016).

2 Shoemaker, C. J. & Green, R. Translation drives mRNA quality control. *Nat Struct Mol Biol* **19**, 594-601, doi:10.1038/nsmb.2301 (2012).

3 Blanco, S. *et al.* Stem cell function and stress response are controlled by protein synthesis. *Nature* **534**, 335-340, doi:10.1038/nature18282 (2016).

4 Signer, R. A., Magee, J. A., Salic, A. & Morrison, S. J. Haematopoietic stem cells require a highly regulated protein synthesis rate. *Nature* **509**, 49-54, doi:10.1038/nature13035 (2014).

5 Guydosh, N. R. & Green, R. Dom34 rescues ribosomes in 3' untranslated regions. *Cell* **156**, 950-962, doi:10.1016/j.cell.2014.02.006 (2014).

6 Rezza, A. *et al.* Signaling Networks among Stem Cell Precursors, Transit-Amplifying Progenitors, and their Niche in Developing Hair Follicles. *Cell Rep* **14**, 3001-3018, doi:10.1016/j.celrep.2016.02.078 (2016).

7 Becker, T. *et al.* Structure of the no-go mRNA decay complex Dom34-Hbs1 bound to a stalled 80S ribosome. *Nat Struct Mol Biol* **18**, 715-720, doi:10.1038/nsmb.2057 (2011).

8 Ishimura, R. *et al.* RNA function. Ribosome stalling induced by mutation of a CNS-specific tRNA causes neurodegeneration. *Science* **345**, 455-459, doi:10.1126/science.1249749 (2014).

9 Kretzschmar, K., Weber, C., Driskell, R. R., Calonje, E. & Watt, F. M. Compartmentalized Epidermal Activation of beta-Catenin Differentially Affects Lineage Reprogramming and Underlies Tumor Heterogeneity. *Cell Rep* **14**, 269-281, doi:10.1016/j.celrep.2015.12.041 (2016).

10 Elkenani, M. *et al.* Pelota Regulates Epidermal Differentiation by Modulating BMP and PI3K/AKT Signaling Pathways. *J Invest Dermatol* **136**, 1664-1671, doi:10.1016/j.jid.2016.04.020 (2016).

11 Florin, L. *et al.* Delayed wound healing and epidermal hyperproliferation in mice lacking JunB in the skin. *J Invest Dermatol* **126**, 902-911, doi:10.1038/sj.jid.5700123 (2006).

12 Young, D. J., Guydosh, N. R., Zhang, F., Hinnebusch, A. G. & Green, R. Rli1/ABCE1 Recycles Terminating Ribosomes and Controls Translation Reinitiation in 3'UTRs In Vivo. *Cell* **162**, 872-884, doi:10.1016/j.cell.2015.07.041 (2015).

13 Mills, E. W., Wangen, J., Green, R. & Ingolia, N. T. Dynamic Regulation of a Ribosome Rescue Pathway in Erythroid Cells and Platelets. *Cell Rep* **17**, 1-10, doi:10.1016/j.celrep.2016.08.088 (2016).

14 Mills, E. W., Green, R. & Ingolia, N. T. Slowed decay of mRNAs enhances platelet specific translation. *Blood* **129**, e38-e48, doi:10.1182/blood-2016-08-736108 (2017).

15 Ingolia, N. T., Brar, G. A., Rouskin, S., McGeachy, A. M. & Weissman, J. S. The ribosome profiling strategy for monitoring translation in vivo by deep sequencing of ribosome-protected mRNA fragments. *Nat Protoc* **7**, 1534-1550, doi:10.1038/nprot.2012.086 (2012).

16 Ingolia, N. T., Lareau, L. F. & Weissman, J. S. Ribosome profiling of mouse embryonic stem cells reveals the complexity and dynamics of mammalian proteomes. *Cell* **147**, 789-802, doi:10.1016/j.cell.2011.10.002 (2011).

17 Guydosh, N. R., Kimmig, P., Walter, P. & Green, R. Regulated Ire1-dependent mRNA decay requires no-go mRNA degradation to maintain endoplasmic reticulum homeostasis in S. pombe. *Elife* **6**, doi:10.7554/eLife.29216 (2017).
18 Guydosh, N. R. & Green, R. Translation of poly(A) tails leads to precise mRNA cleavage. *RNA* **23**, 749-761, doi:10.1261/rna.060418.116 (2017).
19 Slevin, M. K. *et al.* Deep sequencing shows multiple oligouridylations are required for 3' to 5' degradation of histone mRNAs on polyribosomes. *Mol Cell* **53**, 1020-1030, doi:10.1016/j.molcel.2014.02.027 (2014).
20 Ben-Shem, A., Jenner, L., Yusupova, G. & Yusupov, M. Crystal structure of the eukaryotic ribosome. *Science* **330**, 1203-1209, doi:10.1126/science.1194294 (2010).
21 Lareau, L. F., Hite, D. H., Hogan, G. J. & Brown, P. O. Distinct stages of the translation elongation cycle revealed by sequencing ribosome-protected mRNA fragments. *Elife* **3**, e01257, doi:10.7554/eLife.01257 (2014).
22 Thoreen, C. C. *et al.* A unifying model for mTORC1-mediated regulation of mRNA translation. *Nature* **485**, 109-113, doi:10.1038/nature11083 (2012).
23 Kristensen, A. R., Gsponer, J. & Foster, L. J. Protein synthesis rate is the predominant regulator of protein expression during differentiation. *Mol Syst Biol* **9**, 689, doi:10.1038/msb.2013.47 (2013).
24 Laplante, M. & Sabatini, D. M. mTOR signaling in growth control and disease. *Cell* **149**, 274-293, doi:10.1016/j.cell.2012.03.017 (2012).
25 Darnell, J. C. *et al.* FMRP stalls ribosomal translocation on mRNAs linked to synaptic function and autism. *Cell* **146**, 247-261, doi:10.1016/j.cell.2011.06.013 (2011).
26 Sawicka, K., Pyronneau, A., Chao, M., Bennett, M. V. & Zukin, R. S. Elevated ERK/p90 ribosomal S6 kinase activity underlies audiogenic seizure susceptibility in fragile X mice. *Proc Natl Acad Sci U S A* **113**, E6290-E6297, doi:10.1073/pnas.1610812113 (2016).
27 Liu, R. *et al.* Impairing the production of ribosomal RNA activates mammalian target of rapamycin complex 1 signalling and downstream translation factors. *Nucleic Acids Res* **42**, 5083-5096, doi:10.1093/nar/gku130 (2014).
28 Mills, E. W. & Green, R. Ribosomopathies: There's strength in numbers. *Science* **358**, doi:10.1126/science.aan2755 (2017).
29 Watt, F. M., Jordan, P. W. & O'Neill, C. H. Cell shape controls terminal differentiation of human epidermal keratinocytes. *Proc Natl Acad Sci U S A* **85**, 5576-5580 (1988).
30 Gingold, H. *et al.* A dual program for translation regulation in cellular proliferation and differentiation. *Cell* **158**, 1281-1292, doi:10.1016/j.cell.2014.08.011 (2014).
31 Page, M. E., Lombard, P., Ng, F., Gottgens, B. & Jensen, K. B. The epidermis comprises autonomous compartments maintained by distinct stem cell populations. *Cell Stem Cell* **13**, 471-482, doi:10.1016/j.stem.2013.07.010 (2013).

Methods

Mouse strains

All mouse experiments were performed under a UK Government Home Office project license and subject to local institutional ethical approval. The generation of conditional *Pelo*$^{fl/fl}$ (*Pelo*^{tm1Imad}) mice was described elsewhere[32]. To derive constitutive *Pelo* epidermal knockout mice (*Pelo*^{epiKO}), *Pelo*$^{fl/fl}$ mice were crossed with *Krt14*^{Cre} mice (Jax strain, stock number 004782). To achieve temporally controlled *Pelo* knockout and genetic labeling of cells lacking *Pelo*, *Pelo*$^{fl/fl}$ mice were crossed with *Krt14*^{CreERT} (Jax strain, stock number 005107), *Lrig1*$^{EGFP\text{-}IRES\text{-}CreERT2}$ mice[31], *Lgr5*$^{EGFP\text{-}IRES\text{-}CreERT2}$ mice[33], *Lgr6*$^{EGFP\text{-}IRES\text{-}CreERT2}$ mice[34] and *Rosa26*$^{LoxP\text{-}Stop\text{-}LoxP\text{-}tdTomato}$ mice[35]. To activate Cre recombinase, 4-Hydroxytamoxifen (4-OHT, Sigma-Aldrich) was dissolved in acetone and applied topically (3 mg/100 µl) every day for five days and once a week for three weeks. For proliferation assays, 5-ethynyl-2′-deoxyuridine (EdU) (Invitrogen, 20 mg kg^{-1} body mass; in PBS) was injected intraperitonially and the tissue was harvested 1 hr later. To derive constitutive *Pelo* dermal knockout mice (*Pelo*^{derKO}), *Pelo*$^{fl/fl}$ mice was crossed with *Dermo1*^{Cre} (B6.129X1-*Twist2*$^{tm1.1(cre)Dor}$/J)[36,37]. Mouse lines used in this study with the location of expression of markers in the skin are illustrated in the Extended Data Fig. 10k. *Hbs1l*$^{-/-}$ (*Hbs1l*$^{tm1a(KOMP)Wtsi}$) mice were produced at the Wellcome Trust Sanger Institute Mouse Genetics Project as part of International Mouse Phenotype Consortium (IMPC)[38].

Library generation for ribosome profiling

Samples of *Pelo*^{epiKO} epidermis for ribosome profiling and RNA-Seq were prepared by scrapping off the epidermal layer in liquid nitrogen. Frozen samples were ground using a Mixer Mill (Retch) and thawed in the presence of polysome lysis buffer. Lysates were clarified by

362 centrifugation at 20,000g for 10 minutes at 4˚C and the supernatant was collected. Total lysate
363 RNA was quantified using the Quant-it RNA kit (Thermo) and 5 µg was used for preparation of
364 ribosome profiling libraries as described previously[15]. Total RNA was size-selected by excising
365 gel regions between phosphorylated 16nt and 34nt RNA oligo standards. Ribosomal RNAs were
366 depleted using Ribo-Zero Gold (Illumina) after footprint size-selection. 100ng was used for
367 preparation of RNA-Sequencing libraries from the same samples as profiling libraries. Analysis
368 using a BioAnalyzer total RNA pico chip was used to confirm RNA integrity (RIN >9) for RNA
369 sequencing samples. The datasets are deposited in GEO under accession number GSE94385.
370
371 **Sequencing and data analysis**
372 Ribosome profiling and RNA-Seq libraries were sequenced using a HiSeq2500 (Illumina). ~110
373 million total raw reads were generated from 4 ribosome profiling samples with between 11 and
374 30 million reads mapping to the genome per sample. For ribosome profiling analysis, only
375 singly-mapped reads (NH:i:1) with no mismatches (NM:I:0) were used. Translational efficiency
376 (TE) was calculated as number of CDS RPFs / RPKM. Relative 3´UTR ribosome occupancy was
377 calculated as 3´UTR footprint density / CDS footprint density. For differential gene expression
378 analysis, we uploaded the list of differentially expressed genes into Ingenuity IPA and ran a core
379 analysis. This identified the top molecules, pathways and master regulators that are different
380 between control and *Pelo*^{epiKO} samples.
381
382 **Polysome analysis**
383 Epidermal layers from WT and *Pelo* ^{epiKO} were lyzed as described above (see Library generation
384 for ribosome profiling). Clarified lysates were loaded on 10-50% sucrose gradients prepared in
385 polysome gradient buffer (20mM Tris-HCl [pH8], 150mM KCl, 5mM $MgCl_2$, 0.5mM DTT,

0.1mg/mL cycloheximide), and gradients were spun in an SW41-Ti rotor at 40,000 rpm for 3 hr at 4°C. Gradients were fractionated using a Brandel Density Gradient Fractionation System. Prior to RNA extraction, CLuc mRNA (NEB) was added in each fraction. RNA was extracted using hot acidic phenol and cDNA was synthesized using iScript cDNA synthesis kit (Bio-Rad) according to manufacturer's instructions. qPCR was carried out using iTaq Universal SYBR Green Supermix (Bio-Rad). Relative mRNA abundances in indicated fractions were normalized to CLuc mRNA to account for differences in RNA extraction efficiency among fractions, and then calculated as fold changes normalized to 80S fractions. qPCR primers: CLuc Forward 5´-GCTTCAACATCACCGTCATTG-3', CLuc Reverse 5'-CACAGAGGCCAGAGATCATTC-3´, Krt86 Forward 5'-AACAGAATGATCCAGAGGCTG–3', Krt86 Reverse 5'-GCTCAGATTGGGTCACGG-3'.

RNA-seq library preparation and analysis

Primary epidermal cell suspension was prepared as previously described[39]. Briefly, cells were harvested from 3 months old 4-OHT treated *Pelo*$^{fl/+}$; *Lrig1*$^{EGFP\text{-}CreERT2}$, *Pelo*$^{fl/+}$; *Lgr5*$^{EGFP\text{-}CreERT2}$, *Pelo*$^{fl/+}$; *Lgr6*$^{EGFP\text{-}CreERT2}$ control mice and *Pelo*$^{fl/fl}$; *Lrig1*$^{EGFP\text{-}CreERT2}$, *Pelo*$^{fl/fl}$; *Lgr5*$^{EGFP\text{-}CreERT2}$, *Pelo*$^{fl/fl}$; *Lgr6*$^{EGFP\text{-}CreERT2}$ *Pelo* mut mice. Total epidermal population was FACS sorted for GFP+ cells on a BD FACSAriaII cell Sorter and 1000 GFP-high cells collected from each population for RNA-seq. Library construction and the strategy for RNA-seq was performed using Smart-seq2 method as reported previously[40]. Fastq files of paired-end reads were uploaded to Galaxy platform[41] and aligned using STAR aligner[42] to *Mus musculus* reference genome (GRCm38/Mm10). BAM files were processed in R using "rnaseqGene" workflow[43]. The data were analysed using the edgeR package. Processed data were mined using IPA Ingenuity

Pathway Analysis (Qiagen). The datasets are deposited in GEO under accession number GSE106246.

Flow cytometry for measurement of cell size, cycle and protein synthesis *in vivo*

To analyse cell size by flow cytometry, epidermal cells were isolated as previously described[39]. Briefly, epidermis was enzymatically separated from dermis with thermolysin (Sigma, 0.25 mg/mL in PBS) overnight at 4°C. Epidermal sheets were processed into single cell suspensions by incubation in DMEM (Gibco) containing DNAse (Sigma, 250 µg/mL) for 20 min at 37°C with shaking. Single cells were labelled according to standard procedures with anti- Integrin α6-Alexa Fluor 647 or FITC (AbSource, 1:20) antibody. To assess the percentage of proliferating epidermal cells, mice were injected with 500µg 5-ethynyl-2'-deoxyuridine (EdU; 2.5mg/mL in PBS) intraperitoneally and back skin was harvested 2 hr later. Cells were isolated as described above and single cell suspensions were stained with the Click-iT EdU Alexa Fluor 488 Flow Cytometry Kit (Invitrogen) according to the manufacturer's suggestions. Cell cycle analysis was performed on a BD LSR Fortessa cell analyser. Proliferating cells that had incorporated EdU were detected in the FITC/Alexa Fluor 488 channel.

To measure protein synthesis *in vivo*, mice received an intraperitoneal injection of O-propargyl-puromycin (OP-P) (Medchem Source or Thermo Fisher (C10459); 50 mg kg^{-1} body mass; pH 6.4–6.6 in PBS). One hour later mice were euthanized and back and tail skin samples were collected. Epidermal dissociation was performed as described above. The staining for detection of protein synthesis was performed according to the manufacturer instructions (Click-iT Plus OPP Protein Synthesis Assay Kit; Thermofisher Scientific). Samples from PBS-injected mice were also stained for detection of protein synthesis and the fluorescence signal was used to

433 determine background labelling. Rates of protein synthesis were calculated as described
434 previously[3]. Briefly, OP-P signals were normalized to whole epidermis after subtracting
435 autofluorescence background. 'Mean OP-Puro fluorescence' reflected fluorescence values for
436 each cell population normalized to whole epidermis. Labelled cells were analysed on a BD
437 LSRFortessa cell analyser. All data were analysed using FlowJo software.
438
439 **Histology, epidermal wholemounts and imaging**
440 For paraffin sections, skin samples were fixed with 10% neutral buffered formalin overnight
441 before paraffin embedding. The tissues were sectioned and stained with haematoxylin and eosin
442 (H&E) and Herovici's stain by conventional methods. For frozen sections, skin samples were
443 embedded on OCT (optimal cutting temperature compound; VWR), sectioned and fixed in 4%
444 PFA for 10 min before staining. Slides were mounted using ProLong Gold anti-fade reagent
445 containing DAPI (Life Technologies) as a nuclear counterstain. Images were acquired using a
446 Hamamatsu slide scanner and analysed using NanoZoomer software (Hamamatsu).

447 The epidermal wholemount labelling procedure was performed as described previously[44,45]. In
448 brief, mouse tail was slit on the ventral side lengthways. Pieces (0.5x0.5 cm^2) of skin were
449 incubated in 5 mM EDTA in PBS at 37 °C for 4 h. Epidermis was gently peeled from dermis as
450 an intact sheet in a proximal to distal direction, corresponding to the orientation of the hairs, and
451 then the epidermis was fixed in 4% paraformaldehyde (PFA; Sigma) for 1 h at room temperature.
452 Fixed epidermal sheets were washed in PBS and stored in PBS containing 0.2% sodium azide at
453 4° C.

454 Confocal image acquisition of stained wholemounts and skin sections were performed using a

Nikon A1 confocal microscope. Images were analysed using NIS Elements (Nikon Instruments Inc.). Photoshop CS5 (Adobe image suite) was used to optimize the images globally for brightness, contrast and colour balance.

Rapamycin treatment

Rapamycin (LC Laboratories, R5000) was dissolved in acetone. Rapamycin treatment groups received topical applications of 500 µl 0.2% Rapamycin on dorsal and tail skin. Vehicle treatment group mice received an equal volume of acetone without rapamycin. Dorsal skin was shaved before the day of treatment.

Wound and TEWL assays

Full-thickness wounds were made on the lower dorsal skin (5mm) or tail (2mm) using punch biopsy (Stiefel) under analgesia and general anaesthesia. The hair on the back was shaved prior to wounding. Wound closure was measured using a Vernier scale. Epidermal barrier function was assessed by testing basal transepidermal water loss (TEWL) on the dorsal skin of mice using a TEWAmeter (Courage and Khazaka, TM210). Measurements were collected for 15–20 seconds when TEWL readings had stabilized, at approximately 30 seconds after the probe collar was placed on the dorsal skin.

Antibodies

Primary antibodies for wholemount and tissue sections were: chicken anti-Krt14 (Covance, SIG2376, 1:500) or directly conjugated (AlexaFluor 555) Krt14 (LL002, in house, 1:200); directly conjugated (AlexaFluor 488) Krt15 (LHK-15, in-house, 1:50); human anti-p63 (SCBT, sc367333, 1:100); rabbit anti-filaggrin (Covance, PRB-417P, 1:100); mouse anti-FASN (SCBT,

sc48357, 1:100); rabbit anti-Ki67 (Novocastra, NCL-Ki67p, 1:500); rabbit anti-Ki67 (abcam, ab16667, 1:500); rabbit anti- Phospho-S6 Ribosomal Protein (Ser235/236) (pS6K, Cell signaling, 2211, 1:200); rabbit anti-P-Cadherin (Cell signaling, 2130, 1:200); rabbit anti-Vimentin (Cell signaling, 5741s, 1:500); rabbit anti-K10 (Covance, PRB-159P, 1:500); FITC conjugated rat anti-CD49f (Integrin □6, Biolegend, 313606, 1:100); goat anti-Lrig1 (R&D Systems, FAB3688G, 1:200); rabbit anti-Scd1 (Cell signaling, 2794s, 1:500); mouse anti-involucrin (SY5, in-house, 1:500); mouse anti-Pankeratin (abcam, ab8068, 1:200); rat anti-CD34 (RAM34, Thermo Fisher, 14-0341-82, 1:200); Rabbit anti-Phospho-4EBP1 (Thr37/46) (Cell Signalling, 236B4, 1:500) AlexaFluor (Life Technologies) dye-conjugated secondary antibodies were used at 1:250 dilutions.

In vitro knockdown, clonogenicity and skin reconstitution assay

Primary human keratinocytes (strain km) were isolated from neonatal foreskin and cultured on mitotically inactivated 3T3-J2 feeder cells in complete FAD medium, containing 1 part Ham's F12 medium and three parts Dulbecco's modified Eagle's medium (DMEM), 10-4 M adenine, 10% (v/v) FBS, 0.5 μg ml-1 hydrocortisone, 5 μg ml-1 insulin, 10-1 M cholera toxin and 10 ng ml-1 EGF, as described previously[46,47]. siRNA mediated gene silencing was performed as described previously[48]. Briefly, keratinocytes were transferred to feeder free conditions in keratinocyte serum-free medium (KSFM) containing 30 μg ml−1 BPE (bovine pituitary extract) and 0.2 ng ml−1 EGF (Gibco) for 2–3 days. Cells were trypsinized at ~70% confluence and resuspended in cell line buffer SF (Lonza). For each 20μl transfection (program FF-113), 2×105 cells were mixed with 1–2μM siRNA duplexes (Silencer select siRNA for *PELO* ID131910, ID131911, ID131912, as well as negative control, Ambion). Transfected cells were incubated at

room temperature for 5–10 min and subsequently resuspended in pre-warmed KSFM. siRNA nucleofections were performed with the Amaxa 16-well shuttle system (Lonza). Alternatively, keratinocytes cells were transfected by using INTERFERin (Polyplus transfections): 36pmol siRNA, 4ul INTERFERin reagent, and 200ul KSFM were mixed in the collagen coated (20ug/ml in PBS, 1h, 37°) 12-well plate and incubated 20min at room temperature. After the incubation, 75, 000 keratinocytes were seeded to the well (final concentration of siRNA 30nM). Medium was changed after 4 hrs and cells were harvested after 48 hrs.

For clonogenicity assays, nucleofected keratinocytes were seeded at low density (100-250 cells per well) on a prepared feeder layer in 6-well plates containing FAD medium. Keratinocytes were maintained in culture for 12 days and then feeders were removed by Versene treatment combined with tapping the culture flask. Once all the feeder cells were washed away, the remaining keratinocytes colonies were fixed with 4% PFA at room temperature for 10 min. Colonies were then stained with 1% Rhodanile Blue (1:1 mixture of Rhodamine B and Nile Blue A (Acros Organics) solution for 15min and washed with distilled water prior to examination. Stained dishes containing keratinocyte colonies were imaged using a Molecular Imager Gel Doc XR+ imaging system (Bio-Rad). Colonies were measured using ImageJ and clonogenicity was calculated as the percentage of plated cells that formed colonies.

For the skin reconstitution assay, pre-confluent keratinocyte cultures (KM passage 3) were disaggregated and transfected either with *PELO* siRNAs or scrambled control siRNAs. 24 hours post-transfection, keratinocytes were collected and reseeded on irradiated de-epidermised human dermis in 6-well Transwell plates with feeders and cultured at the air–liquid interface for three

524 weeks[49]. Organotypic cultures were fixed in 10% neutral buffered formalin (overnight), paraffin
525 embedded and sectioned for H&E and immunofluorescence analysis.

526

527 **Picrosirius birefringence and dermal thickness and cell density**

528 12µm paraffin sections were stained with picrosirius red using a standard method[50]. Briefly, the
529 sections were de-paraffinized, washed twice with water and stained 1 hr in picrosirius red
530 solution (0.1% Sirius red F3B in saturated aqueous solution of picric acid). After the staining,
531 sections were washed twice with acidified water (0.5 % acetic acid), dehydrated, cleared with
532 xylene, and mounted with DPX mounting medium. The images were acquired using Zeiss
533 Axiophot microscope and AxioCam HRc camera under plane-polarized light. The quantification
534 of total collagen fibers was performed by Fiji (ImageJ) software. The collagen pixels were
535 selected by Color Treshold tool (Hue 0-100, Saturation 0-255 and Brightness 230-255).
536 Thickness of dermis was quantified by NanoZoomer Digital Pathology software (Hamamatsu).
537 The number of cells was determined with ImageJ by counting the nucleus in DAPI stained tissue
538 sections.

539

540 **Statistics**

541 Statistical significance in all experiments was calculated by Student's *t* test. Data are represented
542 as mean ±SEM (error bars). GraphPad Prism was used for calculation and illustration of graphs.

543

544 **Data Availability**

545 All experimental data generated during/and or analysed this study are included in this published
546 article (and its supplementary information files). In addition, ribosome profiling data (accession
547 number GSE94385) and RNAseq data (accession number GSE106246) are available in GEO.

References cited in Methods

32 Nyamsuren, G. *et al.* Pelota regulates the development of extraembryonic endoderm through activation of bone morphogenetic protein (BMP) signaling. *Stem Cell Res* **13**, 61-74, doi:10.1016/j.scr.2014.04.011 (2014).

33 Barker, N. *et al.* Identification of stem cells in small intestine and colon by marker gene Lgr5. *Nature* **449**, 1003-1007, doi:10.1038/nature06196 (2007).

34 Snippert, H. J. *et al.* Lgr6 marks stem cells in the hair follicle that generate all cell lineages of the skin. *Science* **327**, 1385-1389, doi:10.1126/science.1184733 (2010).

35 Madisen, L. *et al.* A robust and high-throughput Cre reporting and characterization system for the whole mouse brain. *Nat Neurosci* **13**, 133-140, doi:10.1038/nn.2467 (2010).

36 Sosic, D., Richardson, J. A., Yu, K., Ornitz, D. M. & Olson, E. N. Twist regulates cytokine gene expression through a negative feedback loop that represses NF-kappaB activity. *Cell* **112**, 169-180 (2003).

37 Lichtenberger, B. M., Mastrogiannaki, M. & Watt, F. M. Epidermal beta-catenin activation remodels the dermis via paracrine signalling to distinct fibroblast lineages. *Nat Commun* **7**, 10537, doi:10.1038/ncomms10537 (2016).

38 Skarnes, W. C. *et al.* A conditional knockout resource for the genome-wide study of mouse gene function. *Nature* **474**, 337-342, doi:10.1038/nature10163 (2011).

39 Jensen, K. B., Driskell, R. R. & Watt, F. M. Assaying proliferation and differentiation capacity of stem cells using disaggregated adult mouse epidermis. *Nat Protoc* **5**, 898-911, doi:10.1038/nprot.2010.39 (2010).

40 Picelli, S. *et al.* Full-length RNA-seq from single cells using Smart-seq2. *Nat Protoc* **9**, 171-181, doi:10.1038/nprot.2014.006 (2014).

41 Afgan, E. *et al.* The Galaxy platform for accessible, reproducible and collaborative biomedical analyses: 2016 update. *Nucleic Acids Res* **44**, W3-W10, doi:10.1093/nar/gkw343 (2016).

42 Dobin, A. *et al.* STAR: ultrafast universal RNA-seq aligner. *Bioinformatics* **29**, 15-21, doi:10.1093/bioinformatics/bts635 (2013).

43 Love, M. I., Anders, S., Kim, V. & Huber, W. RNA-Seq workflow: gene-level exploratory analysis and differential expression. *F1000Res* **4**, 1070, doi:10.12688/f1000research.7035.1 (2015).

44 Braun, K. M. *et al.* Manipulation of stem cell proliferation and lineage commitment: visualisation of label-retaining cells in wholemounts of mouse epidermis. *Development* **130**, 5241-5255, doi:10.1242/dev.00703 (2003).

45 Liakath-Ali, K. *et al.* Novel skin phenotypes revealed by a genome-wide mouse reverse genetic screen. *Nat Commun* **5**, 3540, doi:10.1038/ncomms4540 (2014).

46 Lowell, S., Jones, P., Le Roux, I., Dunne, J. & Watt, F. M. Stimulation of human epidermal differentiation by delta-notch signalling at the boundaries of stem-cell clusters. *Curr Biol* **10**, 491-500 (2000).

47 Gandarillas, A. & Watt, F. M. Changes in expression of members of the fos and jun families and myc network during terminal differentiation of human keratinocytes. *Oncogene* **11**, 1403-1407 (1995).

48 Mulder, K. W. *et al.* Diverse epigenetic strategies interact to control epidermal differentiation. *Nat Cell Biol* **14**, 753-763, doi:10.1038/ncb2520 (2012).

49 Sen, G. L., Reuter, J. A., Webster, D. E., Zhu, L. & Khavari, P. A. DNMT1 maintains progenitor function in self-renewing somatic tissue. *Nature* **463**, 563-567, doi:10.1038/nature08683 (2010).
50 Lattouf, R. *et al.* Picrosirius red staining: a useful tool to appraise collagen networks in normal and pathological tissues. *J Histochem Cytochem* **62**, 751-758, doi:10.1369/0022155414545787 (2014).

Extended Data Figure 1. *Pelo* is expressed in all skin cell subpopulations and Knockout of *Hbs1l* leads to mild dermal phenotype (a, b) *Pelo* and *Hbs1l* are ubiquitously expressed in all cell populations of embryonic and neonatal skin. mRNA expression data obtained from hair and skin gene expression library (Hair-GEL; www.hair-gel.net). (c) Schematic of *Hbs1l* knockout-first allele. (d) Immunolabelling of tail epidermal wholemounts with antibodies to Krt14, Krt15, Lrig1 and FASN. (e) Tail skin sections immunolabelled for Ki67, showing no significant change in the distribution of Ki67+ cells in $Hbs1l^{-/-}$ epidermis. (f) H&E staining of adult control and $Hbs1l^{-/-}$ tail skin. (g) Herovici's polychrome staining to visualize immature (blue) and mature (pink) dermal collagen. (h) Picrosirius staining of tail skin showing the birefringence of collagen fibers against a black background. (i) Immunostaining of tail skin sections with pan-keratin (PanKrt) and vimentin (Vim) antibodies. (j-m) Quantification of dermal thickness (j), dermal cell density (k), dermal cellularity (l) and total collagen deposition (m). Dashed lines mark epidermal-dermal boundary. Scale bars 100 μm. $*p = 0.0286$ in (j, m). n=12 sections analyzed over 4 mice per group. FKPM - Fragments per Kilobase of transcript Per Million mapped reads.

Extended Data Figure 2. Delayed wound closure in *Pelo* null epidermis (a) Histology of skin 10 days post wound (dpw) shows delayed wound closure in $Pelo^{epiKO}$. (b, c) EdU staining of 10 dpw skin shows reduced proliferation in wound bed. Itgα6 staining demarcates dermal-epidermal boundary, Box indicates the wound bed (d) Histology of 5 dpw wound shows altered epidermal architecture. (e, f) EdU labelling of 5 dpw skin shows reduced proliferation at wound

edge. (g, h) Immunostaining of Krt14 in 10 and 5 dpw skin shows abnormal differentiation in *Pelo*^{epiKO} (arrows). (i) TdTomato genetic labeling shows the contribution of Lrig1, Lgr5 and Lgr6 progeny in tail wound healing. Note that altered migration of Lrig1 cells in *Pelo*$^{fl/fl}$; *Lrig1*^{CreERT}; tdTom when compared to Lgr5 and Lgr6 on *Pelo* deletion. *p = 0.0123 in (c), *p = 0.0330 in (e), n=9 sections analyzed over 3 mice per group. Scale bars, 100 μm.

Extended Data Figure 3. *Pelo* deletion leads to progressive hair follicle and sebaceous gland abnormalities (a, b, c) Confocal images of tail epidermal wholemounts immunostained for Krt14, hair follicle bulge markers CD34 and Krt15, sebocyte maturation marker Fatty acid synthase (FASN) and junctional zone stem cell marker Lrig1 show progressive changes in hair follicle and sebaceous gland structure from P16 to P120 in *Pelo*^{epiKO} mice. Note that the FASN staining in P84 and P120 *Pelo*^{epiKO} epidermis is non-specific due to highly keratinized hair follicles. Asterisks in (b) indicate non-specific staining of sebaceous glands. Scale bars, 100 μm.

Extended Data Figure 4. Postnatal epidermal *Pelo* deletion impairs barrier function and wound healing (a, b) Breeding scheme and topical Tamoxifen (4-OHT) treatment regime. (c) Representative *Pelo*$^{fl/fl}$; *Krt14*^{CreERT} mouse showing skin lesions (dashed area) in 4-OHT-treated dorsal skin. (d) TEWL is increased in 4-OHT-treated skin of *Pelo*$^{fl/fl}$; *Krt14*^{CreERT}mice. (e) Rate of wound closure. (f) Tail epidermal wholemounts immunostained with Krt14 and Krt15 antibodies showing altered sebaceous gland architecture (arrows) in 4-OHT-treated *Pelo*$^{fl/fl}$; *Krt14*^{CreERT} mice. (g) Tail epidermal wholemounts from TdTomato (red) genetically labelled *Pelo*$^{fl/fl}$; *Krt14*^{CreERT} mice show keratinized cysts in hair follicles (arrows). (h) Cumulative mean values of gene expression obtained from ribosome profiling show down-regulation of markers of

643 sebaceous gland differentiation and increase in Myc. (i) Tail epidermal wholemounts showing
644 altered expression of FASN, Scd1 and Lrig1 (arrows) in sebaceous glands of 4-OHT-treated
645 *Pelo*$^{fl/fl}$; *Krt14*^{CreERT} mice (middle and right panels). Dashed lines indicate pilosebaceous units.
646 Scale bars, 100 μm. **p = 0.0072, *p = 0.0650, n. s., non significant. n = 3 in treated and
647 untreated control groups.
648
649 **Extended Data Figure 5. Knockdown of *PELO* in human keratinocytes phenocopies mouse**
650 **epidermal phenotype and proliferation difference in mice lacking Pelo in Lrig1, Lgr5 and**
651 **Lgr6 stem cells.** (a-d) PELO knockdown validation. (a) qRT-PCR for individual siRNAs
652 transfected in human primary keratinocytes. (b) Clonal growth. (c, d) colony number and average
653 size of individual colonies. (e-g) Clonal growth of keratinocytes, comparing pooled *PELO*
654 siRNA knockdown (*PELO*^{siRNA}) and scrambled (Scr) control. (h-l) Effect of *PELO* knockdown
655 in human epidermal reconstitution assay on decellularised dermis. (h, i) Epidermal thickness of
656 DED cultures is significantly increased on *PELO* knockdown. (j-l) Immunolabelling for Krt14
657 (K14), Ki67, p63 and differentiation markers Krt10 (K10) and involucrin (IVL) shows increased
658 number of differentiated cell layers (j) and increased number of cells expressing Ki67 and p63
659 (k, l) in *PELO*^{siRNA} reconstituted epidermis. Dashed lines indicated dermal-epidermal boundary.
660 Assessing proliferation by Ki67 and p63 in the dorsal skin IFE sections of mice lacking *Pelo* in
661 Lrig1, Lgr5 and Lgr6 stem cells. Scale bars, 100 μm. ***p = 0.0009 (a, for siRNA#10), ***p =
662 0.0004 (a, for siRNA#11), **p = 0031 (a, for siRNA#12); *p = 0.0286 (c); *p = 0.0286 (d); **p
663 = 0.0022 (f); **p = 0.0087 (g); ****p = < 0.0001 (i); *p = 0.0229 for Ki67 and *p = 0.0107 for
664 p63 (l). n = 2 independent transfections; n = 3 dishes (a - g) and n = 2 sections of reconstituted
665 epidermis (h, l).

Extended Data Figure 6. Lrig1+ stem cells account for *Pelo* mutant epidermal phenotype (a) Tail epidermal wholemounts labeled with Krt14 and Ki67 antibodies, showing increased proliferation and alterations to the junctional zone (asterisks) and sebaceous glands (arrow) in *Pelo*$^{fl/fl}$; *Lrig1*^{CreERT2} mice. (b) Cross section of dorsal skin stained for EdU shows increased proliferation and alterations in HF infundibulum structure (arrow) in *Pelo*$^{fl/fl}$; *Lrig1*^{CreERT2} mice. (c-e) Confocal images of tail epidermal wholemounts (c, e) and dorsal skin sections (d) of tdTomato labelled *Pelo*$^{fl/fl}$; *Lrig1*^{CreERT2}, *Pelo*$^{fl/fl}$; *Lgr5*^{CreERT2} and *Pelo*$^{fl/fl}$; *Lgr6*^{CreERT2} mice. (c, d) Expansion of tdTomato-labelled Lrig1 (arrows) but not Lgr5 or Lgr6 progeny upon *Pelo* deletion. (e, f) Increase in proliferation (Ki67 labelling) of Lrig1 (arrows) but not Lgr5 and Lgr6 populations. Scale bars, 100 μm. *p = 0.0047 (f). n=9 wholemounts analyzed over 3 mice per group. All mice were in telogen of the hair cycle (2-3 months old) when treated with 4-OHT. Treatment regime and harvest of tissue were as indicated in Fig. 2c. Dashed lines mark epidermal-dermal boundary.

Extended Data Figure 7. *Pelo* knockout epidermal cells do not accumulate 3´UTR footprints (a) Empiric cumulative distribution plots of relative 3´UTR ribosome occupancy for all transcripts or (b) those with at least 1 read mapped to the 3´UTR. (c-e) Gene Ontology of genes differentially expressed in *Pelo*-null epidermis. Functional, component and process categories of genes enriched in *Pelo*^{epiKO}.

Extended Data Figure 8. Computational analysis of differentially regulated pathways between control and *Pelo*^{epiKO} and comparison of molecular signatures in *Pelo*^{epiKO} and Gtpbp2-deficient brain (a) Number of genes that were differentially expressed in *Pelo*^{epiKO} and

control epidermis and their associated functions. (b, c) Ingenuity Pathway Analysis showing changes in mTOR pathway genes in *Pelo*^{epiKO} vs control epidermis (b) and their predicted molecular activities (c). (d) Venn diagram shows common differentially expressed genes in our study and that of Ishimura et al (2014) when comparing Ctrl and mutants. The 314 overlapping genes are enriched in top canonical pathways that are highly related to translation.

Extended Data Figure 9. *Pelo* epidermal deletion results in increased protein synthesis and basal stem cell size and Rapamycin treatment reduces proliferation of *Pelo*-null epidermis

(a) Gating strategy for measurement of OP-Puromycin incorporation in cell populations (b, c) Confocal images of tail and ear epidermal wholemounts immunolabelled for Krt14 and P-cadherin (P-Cad), showing IFE basal cells. (d, e) Representative flow cytometric dot plot showing increased cell size (FSC-A) of Itgα6^{high} cells and altered S and G2/M cell cycle phases in *Pelo*^{epiKO} epidermis. (f, g) Breeding scheme and rapamycin treatment regime. (h) Immunolabelling of tail epidermal wholemounts with Krt14 and Ki67 antibodies shows reduced proliferation in rapamycin-treated mice compared to vehicle-treated group. Note that there was no significant change in epidermal proliferation of control mice treated with rapamycin when compared to vehicle treated mice. (i, j) Cross sections of IFE from *Pelo*^{epiKO} and control back skin immunolabelled with Krt14 and Ki67 antibodies, showing significant reduction in Ki67+ and suprabasal Krt14+ cells in rapamycin-treated compared to vehicle-treated mice. (k) Cross sections of IFE from control and *Pelo*^{epiKO} back skin immunolabelled with Krt14 and pS6K antibodies showing marked increase in pS6K labeling indicating mTOR hyperactivation in vehicle-treated *Pelo*^{epiKO} skin. (l) Cross sections of IFE of control and *Pelo*$^{fl/fl}$; *Krt14*^{CreERT} mice (with simultaneous 4-OHT and Rapamycin treatment) immunolabelled for Krt14 and EdU

showing significant reduction in EdU+ and suprabasal Krt14+ cells in rapamycin-treated compared to vehicle-treated mice. (m) Cross sections of IFE of control and *Pelo*$^{fl/fl}$; *Krt14*^{CreERT} mice (with simultaneous 4-OHT and Rapamycin treatment) immunolabelled for Krt14 and p4EBP antibodies. Note reduced pS6K labeling (k) and p4EBP1 (m) in rapamycin-treated epidermis. Gray scale images for pS6K are shown below merged images. Scale bars, 100 μm. *p = 0.0132 in (j), n. s., non significant. n=9 sections analyzed over 3 mice per group. Dashed lines mark epidermal-dermal boundary.

Extended Data Figure 10. RNA-sequencing of Lrig1+, Lgr5+ and Lgr6+ cells reveals Lgr5 as a transcriptionally unique subpopulation and subtle changes in transcription in all subpopulations when *Pelo* is deleted. (a) Schematic illustration of the EGFP^{high} sorting and RNA-seq strategy for control and *Pelo*-deleted subpopulations using *Pelo*$^{fl/fl}$; *Lrig1*$^{EGFP-CreERT2}$, *Pelo*$^{fl/fl}$; L*gr5*$^{EGFP-CreERT2}$ and *Pelo*$^{fl/fl}$; *Lgr6*$^{EGFP-CreERT2}$ mice. (b) Principal component analysis of RNA-seq data shows that the Lgr5 subpopulation is remarkably different from the other two. Note that there is no major change in the clusters when *Pelo* is deleted in any of the subpopulations. (c) Hierarchical clustering of the subpopulations corroborates minimal transcriptional changes between control and Mut mice, revealing two major clusters, one for Lgr5 and another for Lrig1 and Lgr6. (d) Venn diagram illustrating the differentially expressed genes in common between the 3 subpopulations when comparing control and Mut. (e) Top differentially regulated transcription factors between Lrig1 and Lgr5 (f), Lgr5 and Lgr6 (g) and Lrig1 and Lgr6 control subpopulations. (h-j) Top differentially regulated canonical pathways between Lrig1 and Lgr5 (h), Lgr5 and Lgr6 (i) and Lrig1 and Lgr6 control subpopulations (j). (k) Schematic of epidermis showing location of marker expression and the various transgenic mice used in this study.

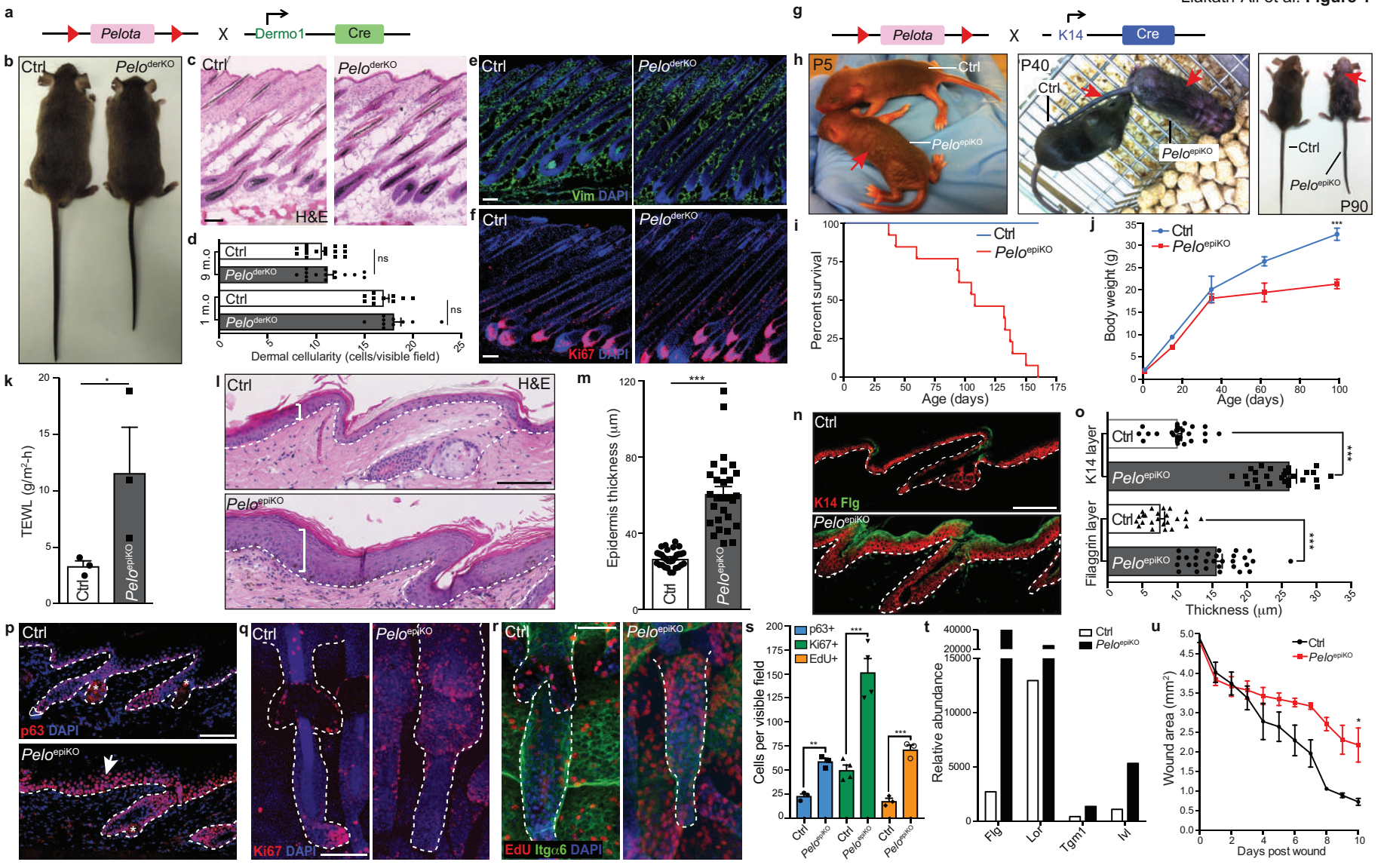
a
Pelota
X
Dermo1
Cre
b
Ctrl
Pelo derKO
c
Ctrl
Pelo derKO
H&E
d
9 m.o
1 m.o
Ctrl
Pelo derKO
ns
Dermal cellularity (cells/visible field)
e
Ctrl
Pelo derKO
Vim DAPI
f
Ctrl
Pelo derKO
Ki67 DAPI
g
Pelota
X
K14
Cre
h
P5
P40
P90
Ctrl
Pelo epiKO
i
Percent survival
Age (days)
j
Body weight (g)
Age (days)
k
TEWL (g/m²-h)
l
Ctrl
Pelo epiKO
H&E
m
Epidermis thickness (μm)
n
Ctrl
Pelo epiKO
K14 Flg
o
K14 layer
Filaggrin layer
Thickness (μm)
p
Ctrl
Pelo epiKO
p63 DAPI
q
Ctrl
Pelo epiKO
Ki67 DAPI
r
Ctrl
Pelo epiKO
EdU Itgα6 DAPI
s
p63+
Ki67+
EdU+
Cells per visible field
t
Ctrl
Pelo epiKO
Relative abundance
Flg
Lor
Tgm1
Ivl
u
Ctrl
Pelo epiKO
Wound area (mm²)
Days post wound

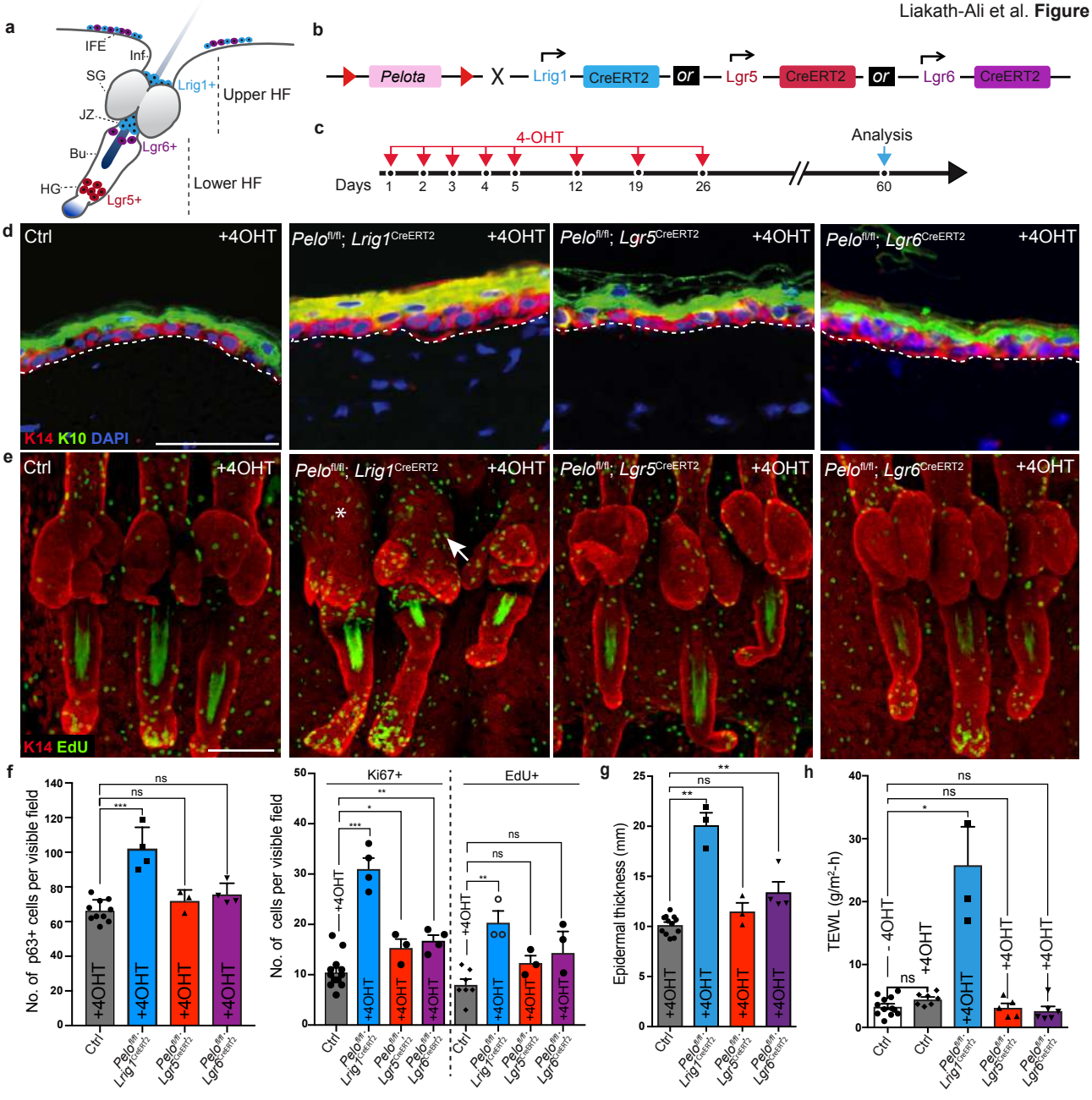
a
IFE
Inf
SG
Lrig1+
Upper HF
JZ
Bu
Lgr6+
HG
Lgr5+
Lower HF
b
Pelota
X
Lrig1
CreERT2
or
Lgr5
CreERT2
or
Lgr6
CreERT2
c
4-OHT
Analysis
Days 1 2 3 4 5 12 19 26 60
d
Ctrl +4OHT
Pelo fl/fl; Lrig1 CreERT2 +4OHT
Pelo fl/fl; Lgr5 CreERT2 +4OHT
Pelo fl/fl; Lgr6 CreERT2 +4OHT
K14 K10 DAPI
e
Ctrl +4OHT
Pelo fl/fl; Lrig1 CreERT2 +4OHT
Pelo fl/fl; Lgr5 CreERT2 +4OHT
Pelo fl/fl; Lgr6 CreERT2 +4OHT
K14 EdU
f
No. of p63+ cells per visible field
No. of cells per visible field
Ki67+
EdU+
+4OHT
Ctrl
Pelo fl/fl; Lrig1 CreERT2
Pelo fl/fl; Lgr5 CreERT2
Pelo fl/fl; Lgr6 CreERT2
ns
g
Epidermal thickness (mm)
h
TEWL (g/m²-h)
- 4OHT
+4OHT

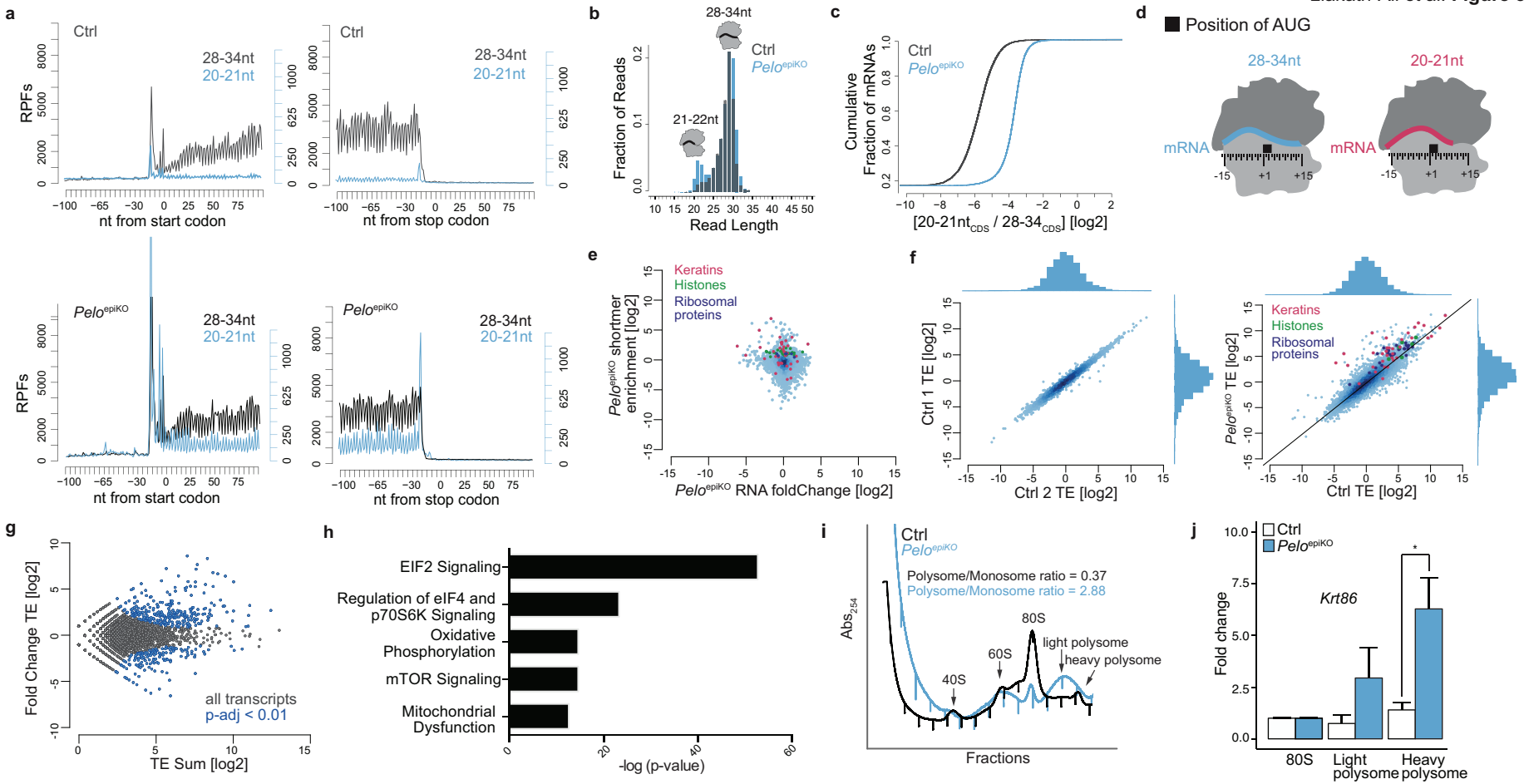
a
Ctrl
28-34nt
20-21nt
RPFs
nt from start codon
nt from stop codon
PeloepiKO
b
28-34nt
21-22nt
Fraction of Reads
Read Length
c
Cumulative Fraction of mRNAs
[20-21nt CDS / 28-34 CDS] [log2]
d
Position of AUG
mRNA
e
Keratins
Histones
Ribosomal proteins
PeloepiKO shortmer enrichment [log2]
PeloepiKO RNA foldChange [log2]
f
Ctrl 1 TE [log2]
Ctrl 2 TE [log2]
PeloepiKO TE [log2]
Ctrl TE [log2]
g
Fold Change TE [log2]
TE Sum [log2]
all transcripts
p-adj < 0.01
h
EIF2 Signaling
Regulation of eIF4 and p70S6K Signaling
Oxidative Phosphorylation
mTOR Signaling
Mitochondrial Dysfunction
-log (p-value)
i
Polysome/Monosome ratio = 0.37
Polysome/Monosome ratio = 2.88
40S
60S
80S
light polysome
heavy polysome
Abs254
Fractions
j
Krt86
Fold change
80S
Light polysome
Heavy polysome

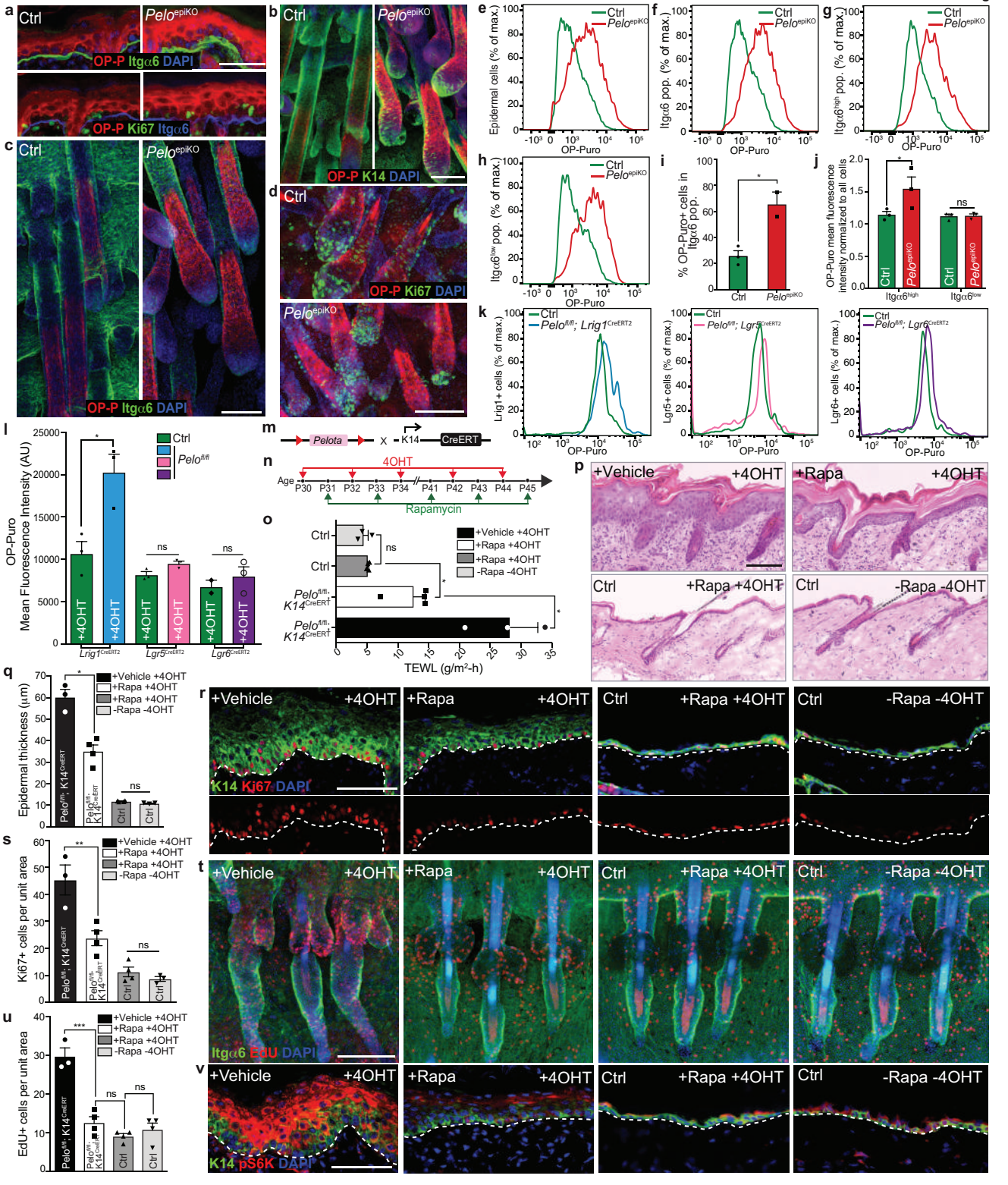
a
Ctrl
Pelo epiKO
OP-P Itgα6 DAPI
OP-P Ki67 Itgα6
b
OP-P K14 DAPI
c
OP-P Itgα6 DAPI
d
OP-P Ki67 DAPI
e
Epidermal cells (% of max.)
OP-Puro
f
Itgα6 pop. (% of max.)
g
Itgα6high pop. (% of max.)
h
Itgα6low pop. (% of max.)
i
% OP-Puro+ cells in Itgα6 pop.
j
OP-Puro mean fluorescence intensity normalized to all cells
Itgα6high
Itgα6low
k
Lrig1+ cells (% of max.)
Lgr5+ cells (% of max.)
Lgr6+ cells (% of max.)
l
OP-Puro Mean Fluorescence Intensity (AU)
+4OHT
Lrig1CreERT2
Lgr5CreERT2
Lgr6CreERT2
m
Pelota
K14
CreERT
n
4OHT
Age
P30 P31 P32 P33 P34 P41 P42 P43 P44 P45
Rapamycin
o
+Vehicle +4OHT
+Rapa +4OHT
-Rapa -4OHT
TEWL (g/m2-h)
p
+Vehicle
+Rapa
Ctrl
q
Epidermal thickness (μm)
r
K14 Ki67 DAPI
s
Ki67+ cells per unit area
t
Itgα6 EdU DAPI
u
EdU+ cells per unit area
v
K14 pS6K DAPI